Aust. J. Phys., 1975, **28**, 185–207

Recombination Lines near 8·9 GHz of Strong Sources in the Southern Milky Way

R. X. McGee, Lynette M. Newton and R. A. Batchelor

Division of Radiophysics, CSIRO, P.O. Box 76, Epping, N.S.W. 2121.

Abstract

Seventeen intense nebulae in the southern Milky Way have been surveyed for their radio recombination lines of hydrogen and helium, H 90α, He 90α, H 113β, H 129γ, and of elements heavier than helium, X 90α. The H 90α line for 30 Doradus in the Large Magellanic Cloud was also observed. Data on source size, flux density, continuum temperature, line temperature, line half-width and radial velocity are used to derive information about the sources. This information includes electron temperatures and turbulent velocities, the abundance ratio of singly ionized helium to ionized hydrogen, and the intensity ratios of β and γ lines to α lines. The lines from elements heavier than helium are discussed.

1. Introduction

The first survey of the radio recombination lines of southern HII regions was made by McGee and Gardner (1968), who investigated 40 sources and found lines in 34. Wilson *et al.* (1970) made a comprehensive search and detected lines in 130 sources. Because of the receiver sensitivities available at the time, both surveys concentrated on the easily detectable α lines. However, 21 sources did reveal β lines (Gardner *et al.* 1970), and a number of cases of southern helium recombination lines were reported (Mezger *et al.* 1970).

Although radio recombination lines were first detected 10 years ago and more than 150 experimental and theoretical papers have been published on the subject, most of the astrophysical conclusions and hypotheses are based on observations of the Orion Nebula, NGC 2024 and IC 1795, and perhaps two or three other sources. The many α-line observations have been used largely for galactic kinematical studies.

In the present survey we have chosen to examine 17 of the more intense southern sources with a telescope beamwidth of $2'\cdot 5$ arc and with a receiver of sensitivity and frequency coverage sufficient to detect a β line (transition of two energy levels) and a γ line (transition of three energy levels) of hydrogen as well as the 90α lines of hydrogen and helium. In a number of cases we have detected lines from elements heavier than helium. The frequencies near 8·9 GHz afforded a useful ratio of line temperature to continuum temperature. The small beam size of the 64 m radio telescope at Parkes gave a better opportunity to explore the origin of the lines than the wider beams of some earlier observations.

2. Equipment and Observational Method

The receiver used was the 3·4 cm wavelength cryogenically cooled instrument described by Kerr (1971). The system temperature on cold sky was 180 K. Calibrations of the system sensitivity and the telescope beamwidth were derived from continuum observations of the radio sources Hydra A, 3C 273, 3C 279 and 1934–63. For most of the observations the half-power beamwidth was $2'\cdot5 \times 2'\cdot5$ arc; for the initial observing session, where conditions of the reflector surface were different, the beam was $2'\cdot6 \times 2'\cdot5$ arc. The telescope pointing accuracy, checked on the four sources observed at a number of zenith angles between 24° and 55°, was $\pm 0'\cdot3$ arc after the effects of beam squint had been eliminated.

An argon discharge tube used for calibrating the intensity scale was itself calibrated against the source Hydra A for which a flux density of 8·0 Jy was assumed (Kellermann and Pauliny-Toth 1971). The relation between full-beam brightness temperature T_b (K) and the flux density S (Jy) of a point source was $S = 1\cdot5\, T_b$.

Observations were made with the multichannel backend, in which the 64 filters with a 3 dB bandwidth of 100 kHz were set at 100 kHz intervals across the receiver band. The observation of a line profile was controlled by a computer program developed by J. C. Ribes (at present at the Observatoire de Paris). The spectrum was displayed on a cathode ray oscilloscope during the integration so that the signal-to-noise improvement was continually monitored. The program arranged for regular intensity calibrations to be applied to each channel. Integrations were continued for a period of 20 min at the source position and for the same period at a reference position having the same declination and initial hour angle. This procedure ensured that zenith angle effects were eliminated when source–reference comparisons were made in the computer. The optimum axial focus of the telescope, which is a function of zenith angle, was adjusted to the best mean value for the integration period. Lateral focusing was required at these frequencies.

In addition to line observations, continuum intensity measurements were necessary. Since these were the first 8·9 GHz observations in the southern sky, continuum sections were obtained for each source by scanning the telescope through the peak intensity in right ascension and declination. From the resulting measurements of half-widths, flux densities of the sources were calculated using the relation

$$S = 1\cdot133\,\Delta w_\alpha \Delta w_\delta (2k/\lambda^2)\, T_{b,\max} = 23\cdot2\,\Delta w_\alpha \Delta w_\delta\, T_{b,\max} \quad \text{Jy}, \tag{1}$$

where w_α and w_δ are the observed widths in minutes of arc at half-intensity of an assumed gaussian-shaped source.

The continuum sections are reproduced in Fig. 1 at the top right-hand side of each line profile; T_c is used to indicate the continuum intensity full-beam brightness temperature, while the right ascension scale is divided into units of 10 s and the declination scale into units of 5′ arc. The observed source half-power widths are marked in angular units on the profiles.

Figs 1*a*–1*q*. Recombination line spectra near a frequency of 8·88 GHz for the 17 nebulae in the southern Milky Way. The ordinates are line temperature T_L in units of full-beam brightness temperature and the abscissae are frequency ν corrected to the local standard of rest (MHz). Equivalent radial velocity (V_r) scales (referred to the local standard of rest) are given below the H 90α, He 90α and H 113β lines. Continuum sections in the directions of right ascension and declination through the positions of the line observations are given as top right insets to the diagrams. The observed widths at half-power are marked in minutes of angle on these profiles.

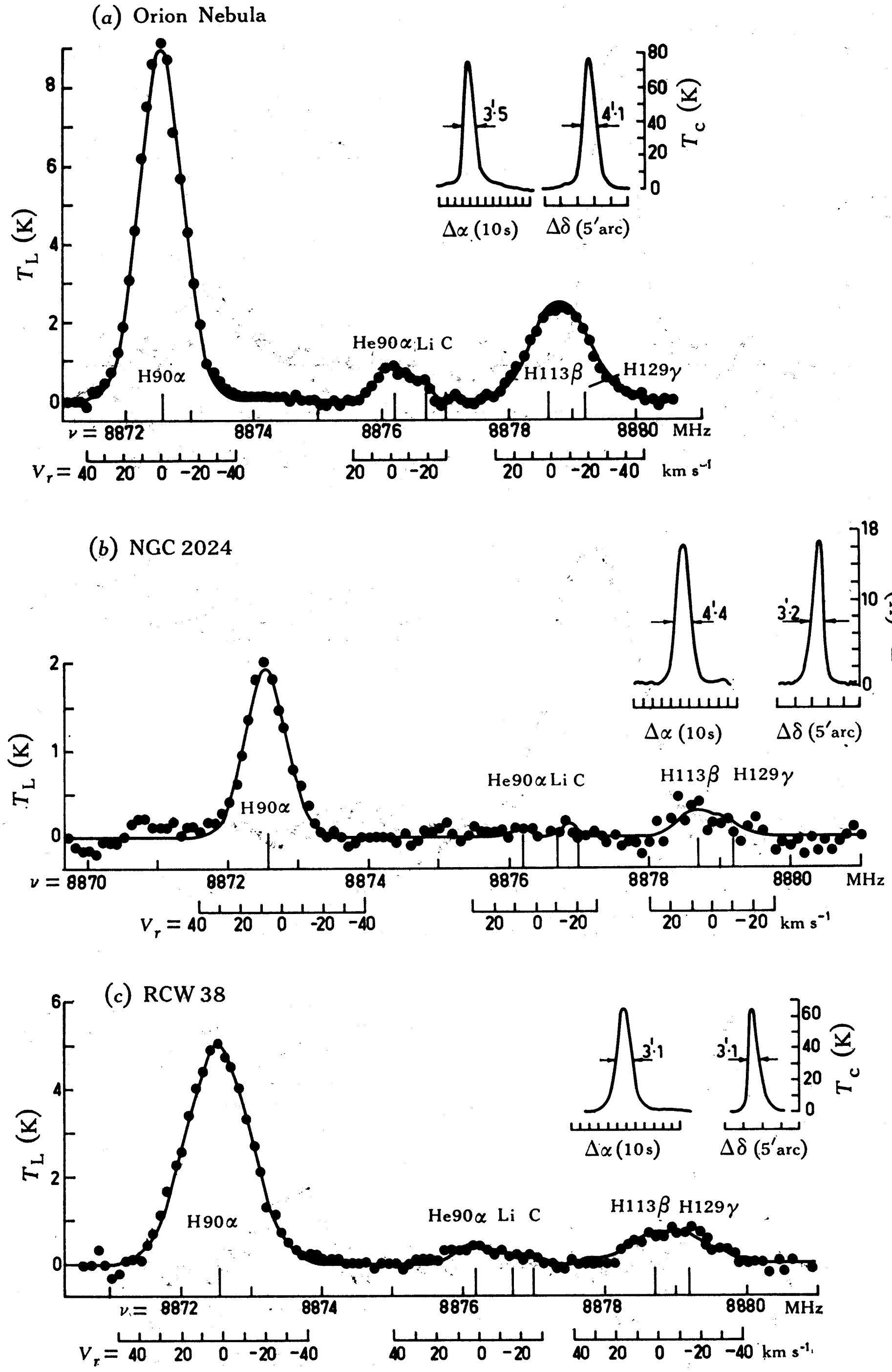
(a) Orion Nebula
T_L (K)
H90α
He90α Li C
H113β
H129γ
ν = 8872
8874
8876
8878
8880 MHz
V_r = 40 20 0 −20 −40
20 0 −20
20 0 −20 −40 km s⁻¹
3'·5
4'·1
T_c (K)
Δα (10s)
Δδ (5'arc)
(b) NGC 2024
T_L (K)
H90α
He90α Li C
H113β H129γ
ν = 8870
8872
8874
8876
8878
8880 MHz
V_r = 40 20 0 −20 −40
20 0 −20
20 0 −20 km s⁻¹
4'·4
3'·2
T_c (K)
Δα (10s)
Δδ (5'arc)
(c) RCW 38
T_L (K)
H90α
He90α Li C
H113β H129γ
ν = 8872
8874
8876
8878
8880 MHz
V_r = 40 20 0 −20 −40
40 20 0 −20
40 20 0 −20 −40 km s⁻¹
3'·1
3'·1
T_c (K)
Δα (10s)
Δδ (5'arc)

Figs 1*a*–1*c*

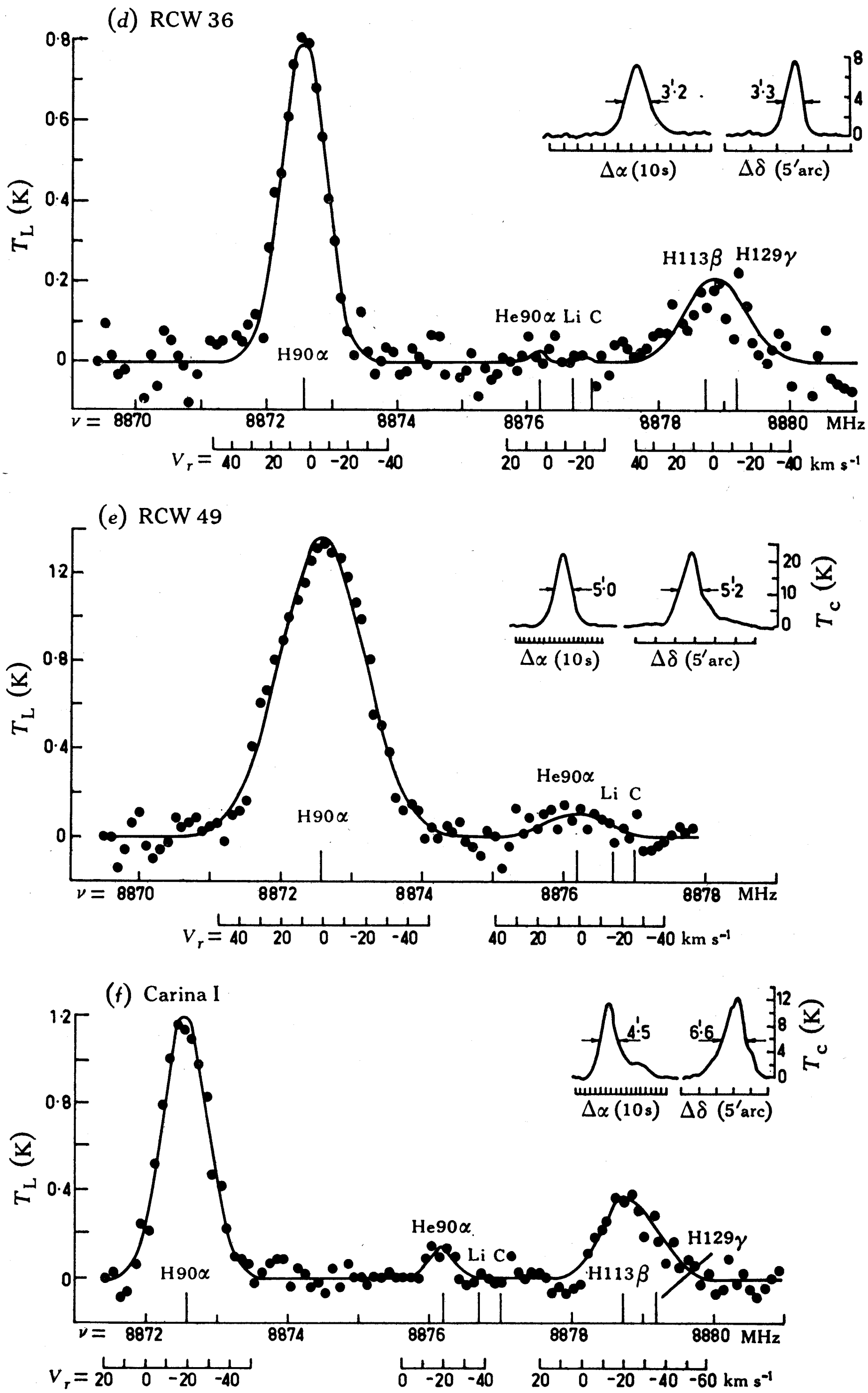
(d) RCW 36
H90α
He90α Li C
H113β H129γ
Δα (10s)
Δδ (5′arc)
3′·2
3′·3
(e) RCW 49
H90α
He90α
Li C
5′·0
5′·2
(f) Carina I
H90α
He90α
Li C
H113β
H129γ
4′·5
6′·6
T_L (K)
T_c (K)
ν = MHz
V_r = km s^{-1}

Figs 1d–1f

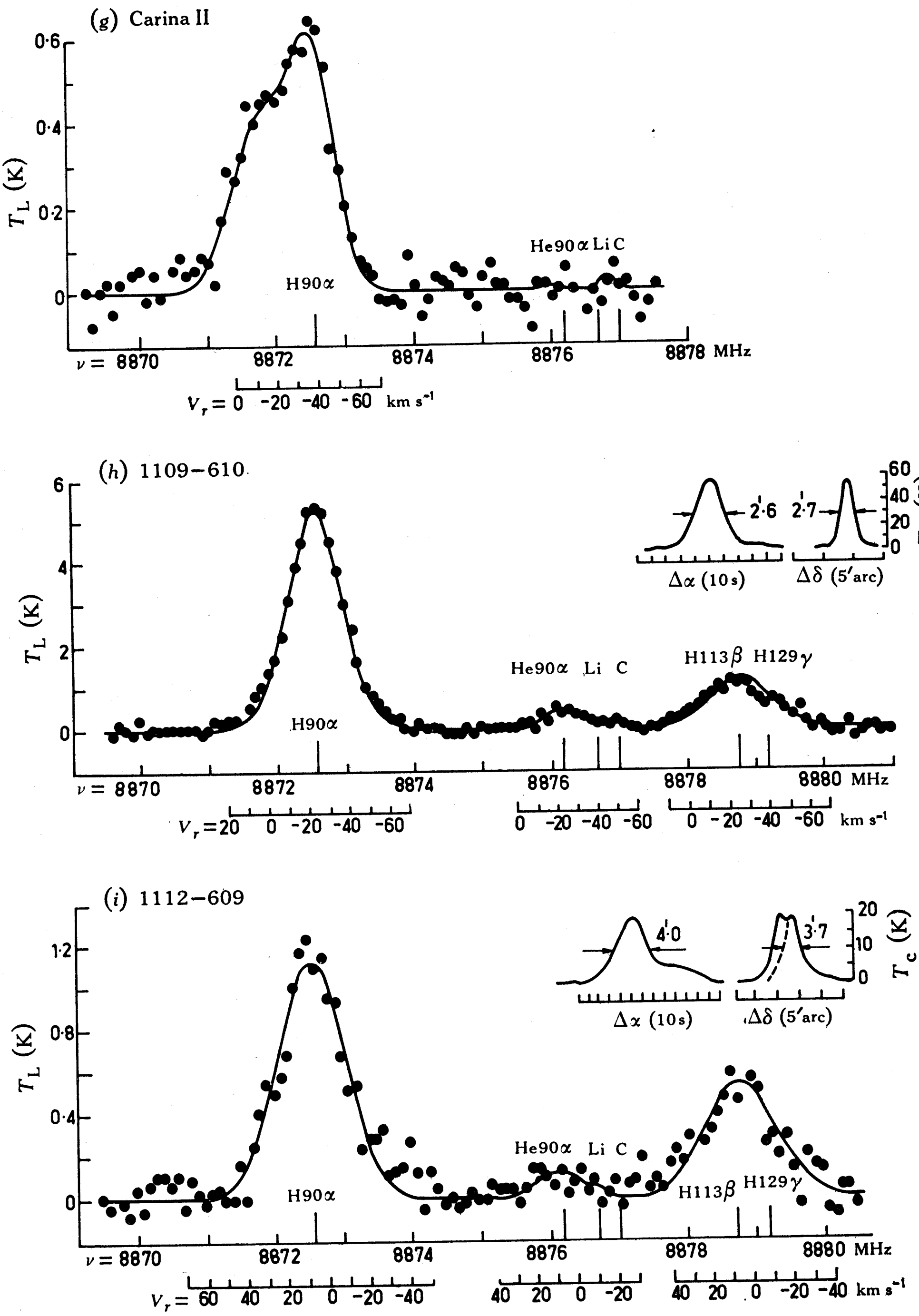
(g) Carina II
0·6
0·4
0·2
0
T_L (K)
He90α Li C
H90α
ν = 8870
8872
8874
8876
8878 MHz
V_r = 0 -20 -40 -60 km s⁻¹
(h) 1109−610
6
4
2
0
T_L (K)
2′·6
2′·7
60
40
20
0
T_c (K)
Δα (10s)
Δδ (5′arc)
He90α Li C
H113β H129γ
H90α
ν = 8870
8872
8874
8876
8878
8880 MHz
V_r=20 0 -20 -40 -60
0 -20 -40 -60
0 -20 -40 -60 km s⁻¹
(i) 1112−609
1·2
0·8
0·4
0
T_L (K)
4′·0
3′·7
20
10
0
T_c (K)
Δα (10s)
Δδ (5′arc)
He90α Li C
H113β H129γ
H90α
ν = 8870
8872
8874
8876
8878
8880 MHz
V_r = 60 40 20 0 -20 -40
40 20 0 -20
40 20 0 -20 -40 km s⁻¹

Figs 1g–1i

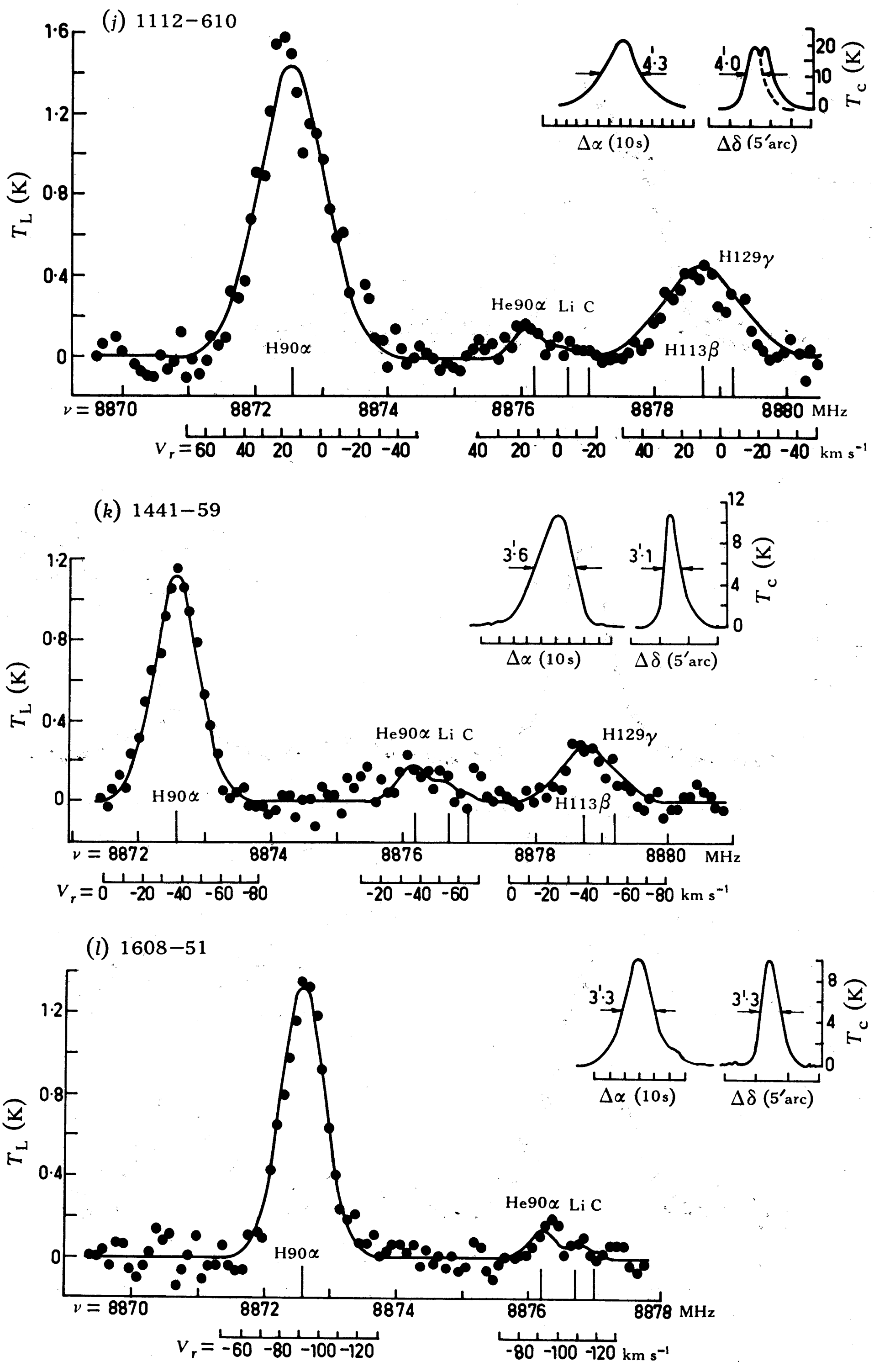
(j) 1112−610
1·6
1·2
0·8
0·4
0
T_L (K)
H90α
He90α Li C
H129γ
H113β
ν = 8870 8872 8874 8876 8878 8880 MHz
V_r = 60 40 20 0 −20 −40
40 20 0 −20
40 20 0 −20 −40 km s⁻¹
4'3
4'0
Δα (10s)
Δδ (5′arc)
20 10 0
T_c (K)
(k) 1441−59
1·2
0·8
0·4
0
T_L (K)
H90α
He90α Li C
H129γ
H113β
ν = 8872 8874 8876 8878 8880 MHz
V_r = 0 −20 −40 −60 −80
−20 −40 −60
0 −20 −40 −60 −80 km s⁻¹
3'6
3'1
Δα (10s)
Δδ (5′arc)
12 8 4 0
T_c (K)
(l) 1608−51
1·2
0·8
0·4
0
T_L (K)
H90α
He90α Li C
ν = 8870 8872 8874 8876 8878 MHz
V_r = −60 −80 −100 −120
−80 −100 −120 km s⁻¹
3'3
3'3
Δα (10s)
Δδ (5′arc)
8 4 0
T_c (K)

Figs 1j–1l

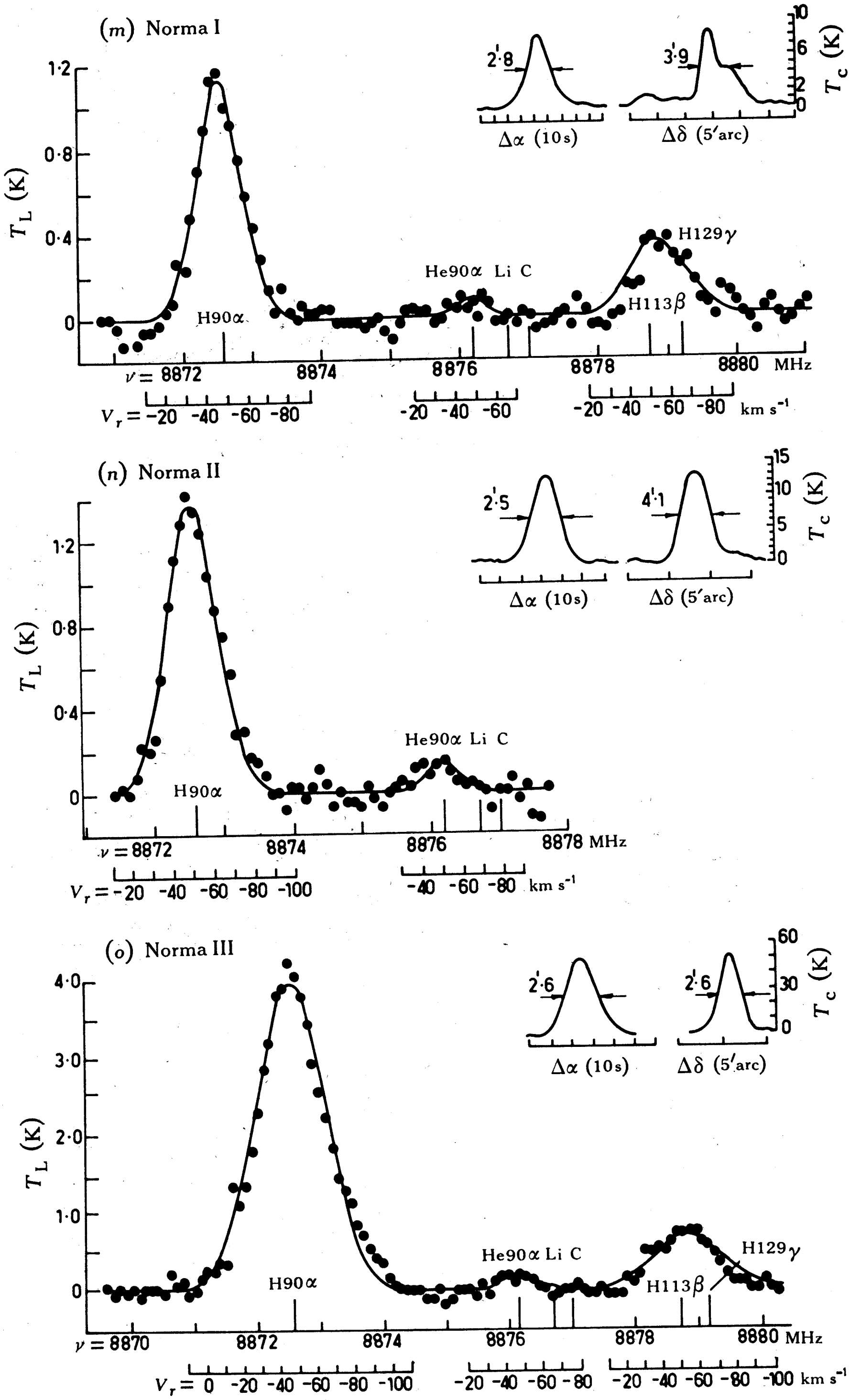
(m) Norma I
(n) Norma II
(o) Norma III
T_L (K)
T_c (K)
H90α
He90α Li C
H113β
H129γ
Δα (10s)
Δδ (5′arc)
2′·8
3′·9
2′·5
4′·1
2′·6
2′·6
ν = 8872
8874
8876
8878
8880 MHz
V_r =
km s⁻¹

Figs 1*m*–1*o*

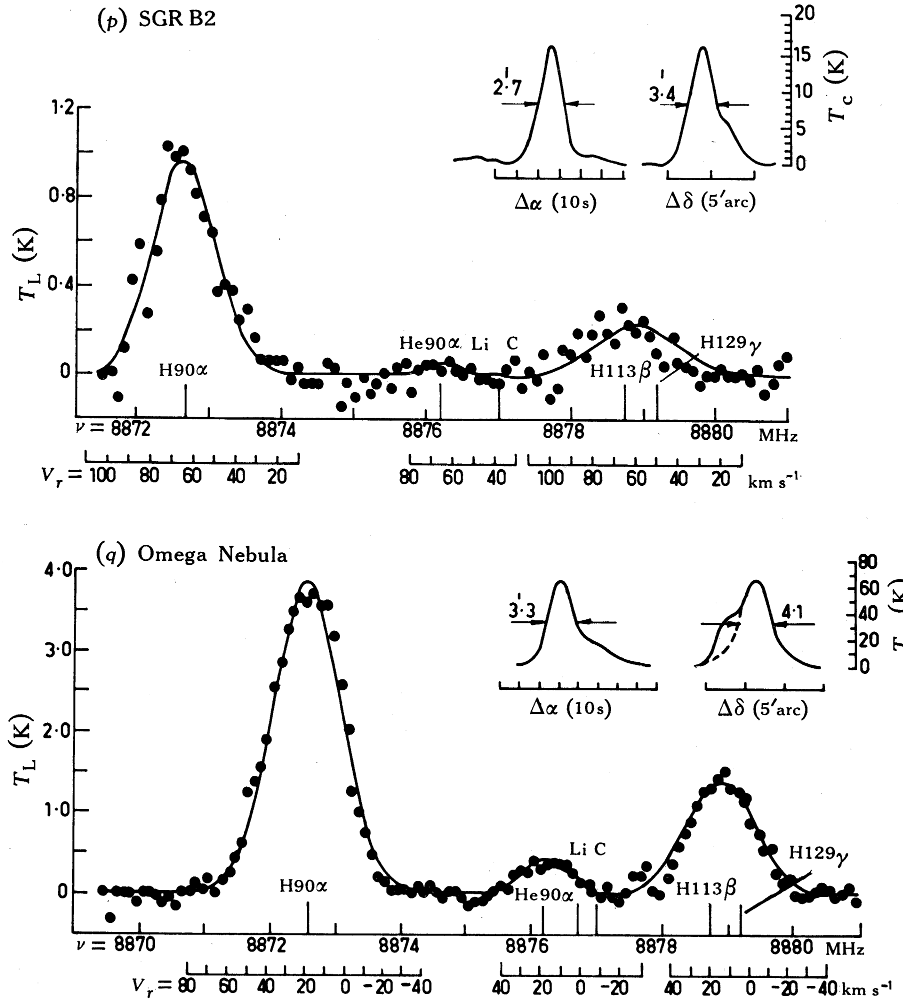

Figs 1*p*, 1*q*

3. Observations

Seventeen sources of the southern Milky Way have been included in the survey. A frequency coverage of approximately 10 MHz in the vicinity of 8·876 GHz has enabled us to detect the recombination lines H 90α, He 90α, H 113β and H 129γ as well as those of other elements near the central frequency. The line profiles produced by overlapping and averaging the complete sets of on–off observations on each source are given in Figs 1*a*–1*q*. It was necessary to overlap sets of 64-point observations centred at appropriate separations in frequency to obtain the full frequency range. Gaussian curves for the recombination lines at various frequencies have been fitted to the points by a computer program. The smooth curves through the dots in Fig. 1 are the resultants of the several gaussians for each source.

The frequency scale was fixed by aligning the rest frequency of the H 90α line (8872·569 MHz) with the centre of the fitted gaussian curve. The first fittings of the He 90α, H 113β and H 129γ lines could then be attempted at their rest frequencies, on the assumption that they were at the same radial velocity as the main hydrogen line. After the iterations in the gaussian-fitting program, the frequency of the helium lines differed from the rest frequency by an average absolute value of $3\cdot4 \pm 3$ kHz and the frequencies of each of the two hydrogen lines (113β and 129γ) by $27\cdot5 \pm 19$ kHz; these errors are well within the limits of the experimental and analytical methods. Since the H 90α, He 90α, H 113β and H 129γ lines have the same radial velocities (within the errors) they may be assumed to emanate from similar regions of the nebulae.

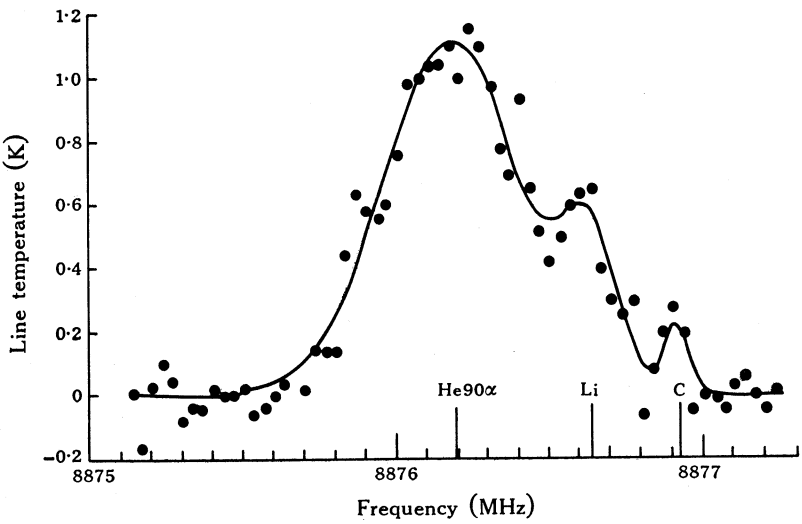

Fig. 2. Spectrum near the He 90α recombination line for the Orion Nebula observed at 33·3 kHz resolution. The line temperature is in units of full-beam brightness temperature. The frequency scale is adjusted so that the centre of the helium line is at the rest frequency of He 90α, namely 8876·184 MHz.

4. Lines near 8·877 GHz

In several cases the profile near helium was asymmetrical about the He 90α frequency; in particular the Orion Nebula, RCW 38, 1109−610, 1112−610, 1441−59 and the Omega Nebula displayed markedly large high-frequency wings. We examined part of the Orion Nebula spectrum with 33·3 kHz filters and obtained the profile shown in Fig. 2. It is now clear that, in addition to the helium line, two higher frequency components are present. Three gaussian curves have been fitted to the points in Fig. 2 in the way described above, and the smooth line represents their resultant. The median of the first line in the wing is 452 kHz higher in frequency than the centre of the He 90α line, while the median of the second is 737 kHz higher. Three interpretations might be considered: the first line could be (*a*) C 90α at a radial velocity of $+9\cdot8\ \mathrm{km\,s^{-1}}$, (*b*) another He 90α line at a more negative radial velocity ($-17\cdot6\ \mathrm{km\,s^{-1}}$) than the main helium line, or (*c*) a line (90α) from one of the elements intermediate between helium and carbon (lithium, beryllium or boron).

Interpretations (*a*) *and* (*b*)

If the first of the higher frequency lines arose from carbon or helium at a different radial velocity, it would seem reasonable to expect a corresponding line of excited hydrogen which would be more easily detectable than the carbon or helium. (This is not necessarily the case with carbon, whose ionization potential of $11\cdot3$ eV is less than that of hydrogen, $13\cdot6$ eV.) There is no evidence of a hydrogen line at either of the required velocities: the residuals from the gaussian-fitted profile to the observed H90α line show no deviations above the noise (Fig. 1*a*). However, possibility (*a*) is the popularly accepted explanation (e.g. Doherty *et al.* 1972; Chaisson 1973*b*). Chaisson used high spectral resolution equivalent to $1\cdot9\ \mathrm{km\,s^{-1}}$ in an unsuccessful attempt to detect a hydrogen component near a velocity of $10\ \mathrm{km\,s^{-1}}$ in the H94α profile which he observed in the Orion Nebula. The situation is further confused by the wider telescope beams of the observations at lower frequencies. For example, Chaisson and Lada (1974) find a radial velocity of $-8\cdot9\ \mathrm{km\,s^{-1}}$ for the H166α line in the Orion Nebula.

The hypothesis that C lines arise in HI regions was based on observations of only three nebulae, the Orion Nebula, NGC 2024 and IC 1795, but it appears to be well supported by low frequency observations. However, in their discussion of the matter Zuckerman and Ball (1974) state that '... data on three (other) better studied sources ... W49 ..., ... W51 ..., and M17 ... are contradictory and otherwise mysterious'. They evolve an elaborate explanation which they summarize thus: 'A comparison of a considerable body of carbon recombination lines and radio molecular line data indicates that these two types of lines (HIα, Cα) are probably formed in dense contiguous regions—the carbon lines in a thin layer facing a hot star and the molecular lines in the rest of the cloud shielded from the stellar radiation by the carbon emitting slab'. We believe that such explanations do not apply in the case of high frequency, high angular-resolution observations of HII regions.

A further complication arises with the carbon or helium interpretation in the case of the Orion Nebula, namely that of identifying the additional line in Fig. 2. Because of these difficulties, we propose a possible alternative explanation.

Interpretation (*c*)

If elements whose lines were closest in radial velocity to those of the hydrogen and helium lines were regarded as possibilities, then the first line in the wing of the Orion Nebula spectrum in Fig. 2 would correspond to Li90α at $-0\cdot2\ \mathrm{km\,s^{-1}}$ and the second to C90α at $+0\cdot2\ \mathrm{km\,s^{-1}}$. The analysis of Fig. 2 is set down in Table 1.

The ionization potential of lithium is $5\cdot39$ eV and hence the observed gas could lie in regions outside the Strömgren sphere of hydrogen. Its abundance from studies of the Sun and meteorites is quite low, with a ratio $N(\mathrm{Li})/N(\mathrm{H}) \approx 10^{-9}$. Two detections of interstellar Li I by means of the $\lambda6708$ Å line have been made in the directions of ζ Oph (Traub and Carleton 1973) and 55 Cygni (Vanden Bout and Grupsmith 1974). In the latter case the authors estimated a ratio $N(\mathrm{Li})/N(\mathrm{H})$ of $2\cdot9\times10^{-10}$ and a column density of lithium of $3\cdot4\times10^{12}\ \mathrm{cm^{-2}}$. We find $N(\mathrm{Li^+})/N(\mathrm{H^+}) \approx 10^{-2}$.

In fitting gaussians to the asymmetrical line profiles associated with He90α in Figs 1 and 2, we have marked the components 'Li' or 'C' depending on whether they were close to the recombination line frequencies for Li 90α or C 90α. We point out that the positioning of these components by the gaussian-fitting program has given line intensities close to the r.m.s. noise in most cases. In the Orion Nebula the positions of these lines deduced from the observations with 100 kHz resolution were slightly different from those deduced from the 33 kHz observation; the narrow C 90α line would have been reduced in amplitude by the 100 kHz filters and was not seen.

Table 1. Spectrum of Orion Nebula near 8·877 GHz with frequency resolution 33·3 kHz
Observations at the continuum maximum, R.A. $05^{\mathrm{h}}\,32^{\mathrm{m}}\,50^{\mathrm{s}}$, Dec. $-05°\,25'\cdot0$ (1950·0)

(1) Line	(2) Rest freq. ν_0 (MHz)	(3) Temp. T_{L} (K)	(4) Half-power width $\Delta\nu$ (kHz)	ΔV (km s^{-1})	(5) $\int T_{\mathrm{L}}\,d\nu$ (K.kHz)	(6) Separation from He 90α (kHz)	(7) Radial velocity (km s^{-1})
He 90α	8876·184	1·12	517	17·5	613	0	−2·3
Li 90α	8876·699	0·46	221	7·5	107	452·3	−0·2
C 90α	8876·995	0·22	87	2·9	20	737·4	+0·2
(H 90α	8872·569	8·88	802	27·1	7574	−3618·7	−2·1)
Estimated errors:		±0·16	±20	±0·7	±3	±15	±0·5

5. Results

The results of the survey are summarized in Table 2, which for convenience of printing has been set down in two parts (*a*) and (*b*). The source size in columns 4 and 5 of Table 2*a* refers to the continuum dimensions. The information given in columns 8–12 is derived from the gaussian-fitting program.

Table 2*b* lists derived parameters. The frequency ν_{obs} of the centre of the fitted line referred to the local standard of rest is given in column 2, followed in column 3 by the difference between the rest line frequency ν_0 and ν_{obs}. The radial velocity V_r (referred to the local standard of rest) at line centre and the difference between the radial velocity of a particular line and that of the H 90α line ($V_r - V_{\mathrm{H}}$) appear in columns 4 and 5. The next three columns 6–8 contain information derived from the line intensities: the ratios $T_{\mathrm{L}}/T_{\mathrm{c}}$ of line temperature to continuum temperature of a source, the quantity $\Delta\nu\, T_{\mathrm{L}}/T_{\mathrm{c}}$, and the integration under a line, $\int T_{\mathrm{L}}\,d\nu$. Five sets of ratios follow in columns 9–13: the ratio $\Delta\nu_{\mathrm{H}}/\Delta\nu_{\mathrm{He}}$ of the half-widths of the H 90α and He 90α lines, the number ratios $N(\mathrm{He}^+)/N(\mathrm{H}^+)$ of helium to hydrogen and $N(\mathrm{Li}^+)/N(\mathrm{H}^+)$ of lithium to hydrogen, which are derived from column 8, and the ratios ($T_{113\beta}/T_{90\alpha}$ and $T_{129\gamma}/T_{90\alpha}$) of the intensities of the β and γ lines to that of the H 90α. The final columns 14 and 15 give radial velocities for formaldehyde lines at frequencies near 4·8 GHz and hydroxyl lines near 1·7 GHz in the directions of these sources. The molecular gas information was kindly supplied before publication by Whiteoak and Gardner (1975).

Observation of H 90α Line in 30 Doradus

While the survey was in progress some limited observations were made of the extragalactic source 30 Doradus in the Large Magellanic Cloud. Profiles of the H 90α

Table 2*a*. Observed parameters

(1) Source	(2) Position (1950) R.A. h m s	(3) Dec. ° ′	(4) Source size $\Delta\alpha$ ′	(5) $\Delta\delta$ ′	(6) Flux $S_{3\cdot4}$ (Jy)	(7) Full beam temp. T_c (K)	(8) Line obs.	(9) Line T_L (K)	(10) Noise r.m.s. (K)	(11) Line half-width $\Delta\nu$ (kHz)	(12) ΔV (km s^{-1})
Orion Nebula (G209·0−19·4)	05 32 50	−05 25·0	2·3	3·2	253±53	76·8±8	H 90α	8·88	0·06	802±10	27·1±0·3
							He 90α	0·88		590±20	19·9±0·7
							Li 90α	0·36		227±20	7·7±0·7
							H 113β	1·93		845±20	28·6±0·7
							H 129γ	1·10		860±20	29·1±0·7
NGC 2024 (G206·5−16·4)	05 39 12	−01 56·0	3·5	2·0	54±11	16·4±2	H 90α	1·88	0·09	699±20	23·6±0·7
							He 90α	0·10		355±100	12·0±3·4
							C 90α	0·15		247±50	8·3±1·7
							H 113β	0·28		661±100	22·3±3·4
							H 129γ	0·10		648±100	21·9±3·4
RCW 38 (G267·9−1·1)	08 57 24	−47 18·8	1·6	1·8	140±29	63·6±6	H 90α	4·95	0·10	1068±10	36·1±0·3
							He 90α	0·40		613±100	20·7±3·4
							Li 90α	0·17		408±80	13·8±2·7
							C 90α	0·12		306±80	10·3±2·7
							H 113β	0·47		1058±100	35·8±3·4
							H 129γ	0·37		1057±100	35·7±3·4
RCW 36 (G265·1+1·5)	08 57 38	−43 33·6	1·8	2·1	18±4	7·5±0·8	H 90α	0·79	0·04	795±20	26·9±0·7
							He 90α	(0·03)		(201)±100	(6·8)±3·4
							C 90α	(0·02)		(197)	(6·7)
							H 113β	0·15		871±200	29·4±6·8
							H 129γ	0·11		879±200	29·7±6·8
RCW 49 (G284·3−0·3)	10 22 16	−57 31·1	4·3	4·6	134±28	22·5±2	H 90α	1·36	0·06	1389±100	46·9±3·4
							He 90α	0·10		1004±100	33·9±3·4
Carina I (G287·4−0·6)	10 41 36	−59 18·9	3·7	6·1	82±17	12·1±1	H 90α	1·19	0·04	744±20	25·2±0·7
							He 90α	0·14		389±80	13·1±2·7
							H 113β	0·31		666±80	22·5±2·7
							H 129γ	0·18		682±80	23·0±2·7
Carina II (G287·6−0·6)	10 42 52	−59 23·5	5·2	4·8	108±23	11·2±1	H 90α(i)	0·54	0·04	756±80	25·6±2·7
							H 90α(ii)	0·40		957±80	32·3±2·7

1109−610 (G294·3−0·7)	11	09	44	−61	02·3	0·2	0·9	92±19	56·0±6	H 90α	5·18	0·08	952±10	32·2±0·3
										He 90α	0·45		639±40	21·6±1·4
										C 90α	0·15		232±80	7·9±2·7
										H 113β	0·97		948±100	32·0±3·4
										H 129γ	0·33		943±100	31·9±3·4
1112−609 (G291·6−0·5)	11	12	48	−60	57·4	3·0	2·7	66±14	19·5±2	H 90α	1·12	0·07	1147±100	38·8±3·4
										He 90α	0·12		759±100	25·6±3·4
										Li 90α	(0·02)		(430)	(14·5)
										H 113β	0·39		1073±100	36·3±3·4
										H 129γ	0·20		1092±100	36·9±3·4
1112−610 (G291·6−0·6)	11	12	57	−61	00·1	3·4	3·0	85±18	21·6±2	H 90α	1·43	0·08	1215±100	41·0±3·4
										He 90α	0·15		511±100	17·3±3·4
										Li 90α	(0·06)		(299)	(10·1)
										C 90α	(0·05)		(204)	(6·9)
										H 113β	0·25		1354±100	45·7±3·4
										H 129γ	0·23		1352±100	45·7±3·4
1441−59 (G316·8−0·1)	14	41	32	−59	36·6	2·5	1·7	27±6	10·6±1	H 90α	1·11	0·05	833±20	28·1±0·7
										He 90α	0·18		537±40	18·2±1·4
										Li 90α	0·08		297±40	10·0±1·4
										C 90α	(0·03)		(196)	(6·6)
										H 113β	0·23		792±50	26·8±1·7
										H 129γ	0·09		770±50	26·0±1·7
1608−51 (G331·5−0·1)	16	08	21	−51	19·3	2·0	2·0	25±5	9·9±1	H 90α	1·32	0·06	768±30	25·9±1·0
										He 90α	0·13		462±100	15·6±3·4
										Li 90α	0·08		314±50	10·6±1·7
										C 90α	(0·04)		(212)	(7·2)
Norma I (G333·1−0·4)	16	17	15	−50	28·4	1·4	3·0	23±5	8·5±1	H 90α	1·12	0·05	779±20	26·3±0·7
										He 90α	0·08		543±80	18·4±2·7
										C 90α	(0·01)		(128)	(4·3)
										H 113β	0·26		764±40	25·8±1·4
										H 129γ	0·16		738±40	24·9±1·4
Norma II (G333·3−0·4)	16	17	45	−50	19·1	0·6	3·2	31±7	13·2±1	H 90α	1·36	0·06	876±20	29·6±0·7
										He 90α	0·13		549±80	18·6±2·7
										Li 90α	(0·02)		(209)	(7·1)

Table 2a (*Continued*)

(1) Source	(2) Position (1950) R.A. h m s	(3) Dec. ° ′	(4) Source size $\Delta\alpha$ ′	(5) $\Delta\delta$ ′	(6) Flux $S_{3\cdot4}$ (Jy)	(7) Full beam temp. T_c (K)	(8) Line obs.	(9) Line T_L (K)	(10) Noise r.m.s. (K)	(11) Line half-width $\Delta\nu$ (kHz)	(12) ΔV (km s^{-1})
Norma III (G333·6−0·2)	16 18 26	−49 58·8	0·9	0·8	80±17	51·3±5	H 90α	3·97	0·07	1282±10	43·3±0·3
							He 90α	0·14		709±100	24·0±3·4
							H 113β	0·44		1109±50	39·5±1·7
							H 129γ	0·30		1155±50	39·0±1·7
Sgr B2 (G0·7−0·0)	17 44 11	−28 21·8	1·0	2·4	34±7	16·3±2	H 90α	0·96	0·05	1054±50	35·6±1·7
							He 90α	0·05		447±100	15·1±3·4
							H 113β	0·13		1182±100	39·9±3·4
							H 129γ	0·12		1198±100	40·5±3·4
Omega Nebula (G15·1−0·7)	18 17 36	−16 12·5	2·2	3·2	208±44	66·9±7	H 90α	3·83	0·11	1220±10	41·2±0·3
							He 90α	0·39		760±40	25·7±1·4
							Li 90α	0·12		198±40	6·7±1·4
							H 113β	0·93		1168±40	39·5±1·4
							H 129γ	0·57		1087±40	36·7±1·4

Table 2b. Derived parameters

(1) Source and line	(2) Observed frequency ν_{obs} (MHz)	(3) Freq. diff. $\nu_0-\nu_{obs}$ (kHz)	(4) V_r at line centre (km s^{-1})	(5) Velocity diff. V_r–V_H (km s^{-1})	(6) $\frac{T_L}{T_c}$ (%)	(7) $\frac{\Delta\nu\,T_L}{T_c}$ (kHz)	(8) $\int T_L\,d\nu$ (K.kHz)	(9) $\frac{\Delta\nu_H}{\Delta\nu_{He}}$	(10) $\frac{N(He^+)}{N(H^+)}$	(11) $\frac{N(Li^+)}{N(H^+)}$	(12) $\frac{T_{113\beta}}{T_{90\alpha}}$	(13) $\frac{T_{129\gamma}}{T_{90\alpha}}$	(14) V_r for H_2CO (km s^{-1})	(15) V_r for OH (km s^{-1})
Orion														
H 90α	8872·569	0	−2·1±0·2	0	11·6	92·7	7574	1·36	0·07	0·011	0·21	0·12	+6·1	—
He 90α	8876·188	−4	−2·3±0·4	−0·2			551							
Li 90α	8876·699	0	−2·1±0·4	0			86							
H 113β	8878·682	+49	−0·5±0·4	1·6			1732							
H 129γ	8879·149	+36	−0·9±0·4	1·2			998							

NGC 2024														
H 90α	8872·569	0	6·6±0·4	0	11·5	80·1	1401	1·97	0·03		0·15	0·05	+9·3 −6·4	+9·3
He 90α	8876·184	0	6·6±1·5	0			36							
C 90α	8876·891	+104	10·2±0·9	3·6			39							
H 113β	8878·709	+22	7·4±1·5	0·8			199							
H 129γ	8879·167	+18	7·3±1·5	0·7			72							
RCW 38														
H 90α	8872·569	0	1·2±0·2	0	7·8	83·1	5622	1·74	0·05	0·013	0·10	0·07	+2·8 +4·4	+1·8
He 90α	8876·183	+1	1·2±1·0	0			263							
Li 90α	8876·698	+1	1·2±0·6	0			74							
C 90α	8876·995	0	1·2±0·6	0			38							
H 113β	8878·732	−1	1·2±1·0	0			527							
H 129γ	8879·187	−2	1·1±1·0	−0·1			418							
RCW 36														
H 90α	8872·569	0	3·0±0·2	0	10·5	83·7	669	—	(0·01)		0·19	0·14	+6·7 +3·7	+5·7
He 90α	8876·182	+2	3·0±1·0	0			7							
C 90α	8876·893	+102	6·4	3·4			3							
H 113β	8878·693	+38	4·3±3·0	1·3			135							
H 129γ	8879·160	+25	3·8±3·0	0·8			104							
RCW 49														
H 90α	8872·569	0	0·9±1·6	0	6·0	84·0	2005	1·38	0·05				−9·5 −14·1	+0·2 −13·1
He 90α	8876·187	−3	0·8±1·6	−0·1			105							
Carina I														
H 90α	8872·569	0	−19·4±0·2	0	9·8	73·2	942	1·91	0·06		0·26	0·15	−23·8	−25·0
He 90α	8876·182	+2	−19·3±1·0	0·1			59							
H 113β	8878·699	+32	−18·3±1·0	1·1			222							
H 129γ	8879·163	+22	−18·7±1·0	0·7			128							
Carina II														
H 90α(i)	8872·569	0	−37·9±1·0	0	4·8	36·4	432							
H 90α(ii)	8871·801	+768	−12·0±1·0	25·9	3·6	34·2	402							

Table 2b (*Continued*)

(1) Source and line	(2) Observed frequency ν_{obs} (MHz)	(3) Freq. diff. $\nu_0-\nu_{obs}$ (kHz)	(4) V_r at line centre (km s^{-1})	(5) Velocity diff. V_r–V_H (km s^{-1})	(6) $\frac{T_L}{T_c}$ (%)	(7) $\frac{\Delta\nu\, T_L}{T_c}$ (kHz)	(8) $\int T_L\, d\nu$ (K.kHz)	(9) $\frac{\Delta\nu_H}{\Delta\nu_{He}}$	(10) $\frac{N(He^+)}{N(H^+)}$	(11) $\frac{N(Li^+)}{N(H^+)}$	(12) $\frac{T_{113\beta}}{T_{90\alpha}}$	(13) $\frac{T_{129\gamma}}{T_{90\alpha}}$	(14) V_r for H_2CO (km s^{-1})	(15) V_r for OH (km s^{-1})
1109–610														
H 90α	8872·569	0	−24·1±0·2	0	9·3	88·1	5245	1·49	0·06		0·19	0·06	−25·8	−25·8
He 90α	8876·187	−3	−24·2±0·4	−0·1			302						−21·6	
C 90α	8876·998	−3	−24·2±0·6	−0·1			37							
H 113β	8878·705	+26	−23·2±0·8	0·9			977							
H 129γ	8879·164	+21	−23·4±0·8	0·7			328							
1112–609														
H 90α	8872·569	0	7·9±1·0	0	5·7	65·9	1369	1·51	0·07	0·007	0·35	0·18	−27·2	+13·1
He 90α	8876·175	+9	8·2±1·0	0·3			93							+15·0
Li 90α	8876·691	+8	8·2±1·0	0·3			9							
H 113β	8878·674	+57	9·8±1·0	1·9			448							
H 129γ	8879·130	+55	9·8±1·0	1·9			236							
1112–610														
H 90α	8872·569	0	14·3±1·0	0	6·6	80·4	1850	2·24	0·04	0·009	0·18	0·16		+13·1
He 90α	8876·172	+12	14·7±1·0	0·4			82							+15·0
Li 90α	8876·687	+12	14·7	0·4			17							
C 90α	8876·983	+12	14·7	0·4			10							
H 113β	8878·676	+55	16·2±1·0	1·9			362							
H 129γ	8879·127	+58	16·3±1·0	2·0			330							
1441–59														
H 90α	8872·569	0	−37·5±0·2	0	10·5	87·2	985	1·55	0·10	0·024	0·21	0·08	−45·9	−38·0
He 90α	8876·179	+5	−37·3±0·4	0·2			102						−37·1	−34·0
Li 90α	8876·683	+16	−37·0±0·4	0·5			24							
C 90α	8876·997	−2	−37·6	−0·1			6							
H 113β	8878·710	+21	−36·8	0·7			197							
H 129γ	8879·192	−7	−37·8±0·5	−0·3			74							

1608−51														
H 90α	8872·569	0	−91·9±0·5	0	13·3	102·4	1074	1·66	0·06	0·026			−89·3	−92·0
He 90α	8876·188	−4	−92·0±1·0	−0·1			66							
Li 90α	8876·703	−4	−92·0±0·5	−0·1			28							
C 90α	8876·999	−4	−92·0	−0·1			9							
Norma I														
H 90α	8872·569	0	−49·0±0·2	0	13·2	102·7	927	1·43	0·05		0·23	0·14	−52·2	−41·8
He 90α	8876·185	−1	−49·0±1·0	0			46							
C 90α	8876·996	−1	−49·0	0			2							
H 113β	8878·765	−34	−50·1±0·5	−1·1			214							
H 129γ	8879·233	−48	−50·6±0·5	−1·6			128							
Norma II														
H 90α	8872·569	0	−51·1±0·3	0	10·3	90·2	1268	1·60	0·06				−53·9	
He 90α	8876·180	+4	−51·0±1·0	−0·1			76							
Li 90α	8876·695	+4	−51·0	−0·1			4							
Norma III														
H 90α	8872·569	0	−47·1±0·2	0	7·7	99·2	5412	1·8	0·02		0·11	0·08	−45·8	−52·0
He 90α	8876·183	+1	−47·1±1·0	0			103							
H 113β	8878·714	+17	−46·5±0·6	0·6			550							
H 129γ	8879·159	+26	−46·2±0·6	0·9			367							
Sgr B2														
H 90α	8872·569	0	62·9±0·5	0	5·9	62·1	1073	2·36	0·02		0·14	0·13	+62·7	+67·3
He 90α	8876·182	+2	63·0±1·0	0·1			23							
H 113β	8878·694	+37	64·1±1·0	1·2			163							
H 129γ	8879·126	+59	64·9±1·0	2·0			153							
Omega														
H 90α	8872·569	0	18·6±0·2	0	5·7	69·8	4973	1·61	0·06	0·005	0·24	0·15	+17·9 +23·7	+19·6
He 90α	8876·187	−3	18·5±0·5	−0·1			318							
Li 90α	8876·702	−3	18·5±0·5	−0·1			25							
H 113β	8878·741	−10	18·3±0·5	−0·3			1154							
H 129γ	8879·192	−7	18·4±0·5	−0·2			663							

lines and the continuum scans in right ascension and declination are shown in Fig. 3. The r.m.s. noise level of 0·05 K was too great to permit the detection of the He 90α line. Details of the observation were as follows.

Position (1950·0)	$05^{h}\,39^{m}\,03^{s}$, $-69°\,07'{\cdot}4$
Size ($\Delta\alpha$, $\Delta\delta$ at half-power)	$<0'{\cdot}3$ arc, $3'{\cdot}6$ arc
Integrated flux density $S_{3\cdot4}$	15 Jy
Peak continuum temperature T_c	5·5 K
Line (H 90α) temperature T_L (ΔT_L r.m.s.)	0·24 K (±0·05 K)
Ratio T_L/T_c	4·4%
Half-width $\Delta\nu$, ΔV	1697 kHz, 57·3 km s^{-1}
Radial velocity (with respect to Sun)	+267·7 km s^{-1}

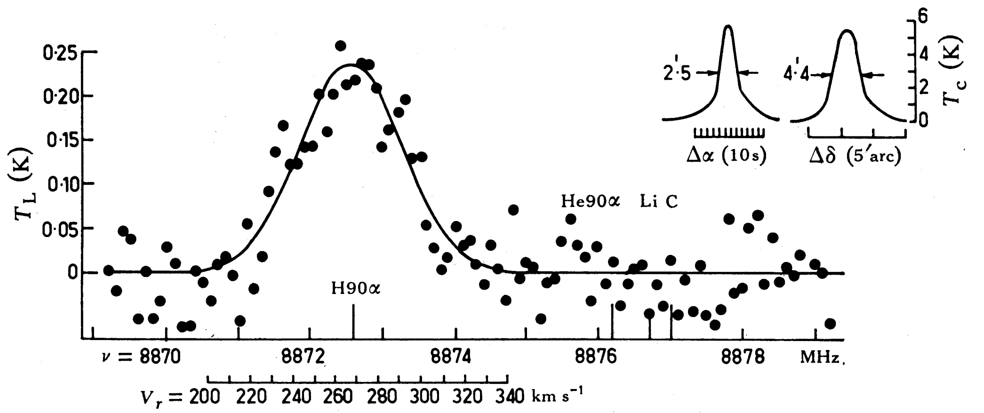

Fig. 3. H 90α recombination line for the 30 Doradus Nebula in the Large Magellanic Cloud. The frequency resolution is 100 kHz. The radial velocity (V_r) scale is referred to the Sun. Continuum sections in the directions of right ascension and declination through the position of the line observations are given in the top right inset.

6. Discussion of Results

Linear Sizes of Sources

It is seen from Table 2*a* that the continuum source sizes are only a few minutes of arc in all cases. We have used the observed radial velocities to calculate the kinematical distances of the sources (in four cases velocities do not fit the model and distances were taken from the literature) and have then converted the angular dimensions into linear sizes. Details are given in Table 3. The average diameter is 3·4 pc, while limiting values are 0·3 and 8·7 pc. Distances lie in the range 0·5–11·9 kpc.

H 90α Lines

The mean value of the ratio of line temperature to continuum temperature in the 17 galactic sources is 8·5±3·0 %, where the error given is the standard deviation. The mean value of the half-widths of the H 90α lines is 963±214(s.d.) kHz. It is difficult to obtain a reliable value of T_L/T_c; the tendency for the wider lines to have a lower T_L/T_c ratio is evident from Tables 2*a* and 2*b*. In the wider profiles it seems possible that two or more recombination lines may be present at different radial velocities because of superposition of sources in the telescope beam. However, the best-fit gaussian analysis does not reveal H 90α lines at radial velocities other than those listed in Table 2*b* in any of the 17 sources under consideration.

He 90α *Lines*

The extremely close agreement in radial velocities of the H 90α and He 90α lines listed in Table 2*b* (the mean of the absolute difference over 16 sources is $0\cdot1\pm0\cdot1$ km s^{-1}) is some evidence that both the hydrogen and helium occupy the same regions of space in the various nebulae.

The relative number abundances of singly ionized helium to ionized hydrogen, given in column 10 of Table 2*b*, have been taken as directly proportional to the ratios of $\int T_L(\nu)\,d\nu$. The sources NGC 2024, RCW 36, Norma III and Sgr B2 have low values, $<0\cdot03$, while the other sources have values in the range 0·04–0·10. The ratio of 0·07 for the Orion Nebula compares with values of 0·074 obtained from Fig. 1 of Churchwell and Mezger (1970) for 109α, 0·083 from Waltman and Johnson (1973) for 66α, 0·067 for 85α and 0·07 for 94α from Chaisson and Ball (1971) and 0·064–0·08 at optical wavelengths from Robbins *et al.* (1971). For NGC 2024 the ratio 0·03 agrees with 0·031 at 94α as obtained by Chaisson (1973a). Column 9 of Table 2*b* indicates that the half-widths of the H 90α lines are considerably greater than those of the He 90α lines. The mean value for the ratio $\Delta\nu_H/\Delta\nu_{He}$ is 1·71.

Table 3. Distances and linear sizes of recombination line sources

Source	Distance (kpc)	Size (pc) Δα	Size (pc) Δδ	Source	Distance (kpc)	Size (pc) Δα	Size (pc) Δδ
Orion Nebula	0·45	0·3	0·4	1112−610	8·76	8·7	7·6
NGC 2024	0·69	0·7	0·4	1441−59	11·92	8·7	5·9
RCW 38	0·65	0·3	0·3	1608−51	6·79	4·0	4·0
RCW 36	0·88	0·5	0·5	Norma I	3·68	1·5	3·2
RCW 49	5·08	6·4	6·8	Norma II	3·84	0·7	3·6
Carina I	(2·7)	2·9	4·8	Norma III	3·58	0·9	0·8
Carina II	(2·7)	4·1	3·8	Sgr B2	(10·0)	2·9	7·0
1109−610	(3·6)	0·2	0·9	Omega Nebula	2·28	1·5	2·1
1112−609	8·17	7·1	6·4				

*H*113β *and H*129γ *Lines*

The natural frequencies of the H113β line (8878·731 MHz) and the H 129γ line (8879·185 MHz) are only 0·454 MHz apart and, since the half-widths in these sources are about 1 MHz, the two are blended. The gaussian-fitting program has been used to place these lines. In Table 2*b* departures from the radial velocity of the H 90α line average less than 1 km s^{-1} for both lines, a value well within experimental error. As expected, the half-widths are close to those of the H 90α lines.

Using the approximations for oscillator strengths given by Menzel (1968) and assuming thermodynamic equilibrium, the ratio of the intensities of the β and α lines and of the γ and α lines may be written:

$$\frac{E_{q+2,q}}{E_{p+1,p}} = \frac{q^3\,\nu_{q+2,q}^3}{p^3\,\nu_{p+1,p}^3}\,\frac{2\cdot633\times10^{-2}\,(1+3/q)}{1\cdot9077\times10^{-1}\,(1+1\cdot5/p)}, \tag{2}$$

$$\frac{E_{r+3,r}}{E_{p+1,p}} = \frac{r^3\,\nu_{r+3,r}^3}{p^3\,\nu_{p+1,p}^3}\,\frac{8\cdot1056\times10^{-3}\,(1+4\cdot5/r)}{1\cdot9077\times10^{-1}\,(1+1\cdot5/p)}, \tag{3}$$

where for the α line $p = 90$ and $\nu_{p+1,p} = 8872\cdot569$ MHz, for the β line $q = 113$

and $\nu_{q+2,q} = 8878\cdot731$ MHz, and for the γ line $r = 129$ and $\nu_{r+3,r} = 8879\cdot158$ MHz. From equation (2) $T_{113\beta}/T_{90\alpha} = 0\cdot276$, and from (3) $T_{129\gamma}/T_{90\alpha} = 0\cdot128$.

Most of the observed β/α ratios fall below those for LTE (local thermodynamic equilibrium) conditions and in almost every case they are similar within experimental errors to the $T_{\mathrm{H}137\beta}/T_{\mathrm{H}109\alpha}$ ratios observed by Gardner *et al.* (1970). On the other hand, seven of the observed γ/α ratios are higher than those for LTE conditions, indicating some unreliability in the estimates. Hjellming and Davies (1970) and Hjellming and Gordon (1970) have used hydrogen α, β, γ, δ and ε line results for a few sources to derive the departures from LTE populations of the levels. The quantity $\Delta\nu\, T_{\mathrm{L}}/T_{\mathrm{c}}$ is plotted against quantum number in the former paper and against frequency in the latter. Our values for the Omega Nebula are close to Hjellming and Davies's observational curve and Hjellming and Gordon's theoretical solution, but those for the Orion Nebula agree less well in the observational case and fall well above the theoretical curves at 8·9 GHz.

Table 4. Calculated values of electron temperature and turbulence

(1) Source	(2) From eq. (4) T_{e} (K)	(3) From eq. (4) V_{t} (km s^{-1})	(4) From eq. (5) T_{e} (K)	(5) From eq. (6) T_{e} (K)	(6) From eq. (6) V_{t} (km s^{-1})
Orion Nebula	7517	19·9	6326	9852	12·4
NGC 2024	7650	10·6	7425	12097	1·5
RCW 38	7440	22·8	7072	25521	8·5
RCW 36	7401	14·4	7269	(15761)	—
RCW 49	7317	31·8	7006	30757	20·7
Carina I	8286	18·5	7832	13420	3·1
1109−610	7090	19·6	6666	16621	12·2
1112−609	9070	24·2	8511	24682	14·2
1112−610	7657	26·9	7339	(36813)	—
1441−59	7148	15·6	6513	13534	9·7
1608−51	6239	14·5	5849	12560	7·3
Norma I	6225	14·9	5882	10414	10·8
Norma II	6950	17·4	6531	15550	9·4
Norma III	6403	29·3	6217	38065	8·5
Sgr B2	9515	21·2	9343	(27703)	—
Omega Nebula	8625	26·6	8162	30394	12·9

Estimation of Electron Temperature and Turbulent Velocities

It has been usual, as a first approximation, to assume low optical depths and LTE conditions in nebulae when estimating electron temperatures and then turbulent velocities. We have calculated the electron temperature T_{e} from three formulae and find that two agree reasonably well while the third produces values which are unrealistically high.

The first formula depends only on the H 90α observations. Values of T_{e} are derived from the expression (see e.g. McGee and Gardner 1968)

$$\frac{T_{\mathrm{L}}\Delta\nu}{T_{\mathrm{c}}} = \left(\frac{4\ln 2}{\pi}\right)^{\frac{1}{2}} \frac{3h^4\, b_{\mathrm{n}}\, un^3\, \nu^3}{16\, mke^4\, T_{\mathrm{e}} \ln[\{(2k)^{3/2}/\pi m^{1/2} e^2 \gamma^{5/2}\}\{T_{\mathrm{e}}^{3/2}/\nu\}]}, \qquad (4)$$

where T_{L}, $\Delta\nu$, T_{c} and ν have already been defined, $b_{\mathrm{n}} = 1$ for LTE, $u = 0\cdot19$ (Menzel 1968) and the quantities h, m, k, e and γ have their usual values. Results for T_{e}

derived from equation (4) and given in column 2 of Table 4 are seen to fall between 6000 and 10 000 K. They are similar to results obtained by Wilson *et al.* (1970) from the H 109α lines: the average difference is 10%.

The availability of the helium-to-hydrogen number density ratio makes it possible to use the formula (see e.g. Lada and Chaisson 1973)

$$\frac{T_{\mathrm{L}}\,\Delta\nu}{T_{\mathrm{e}}} = \frac{2\cdot036\times10^4}{\alpha(\nu,T_{\mathrm{e}})}\left(\frac{6f\nu^{2\cdot1}\,T_{\mathrm{e}}^{-1\cdot15}}{n}\right)\left\{1+\frac{N(\mathrm{He}^+)}{N(\mathrm{H}^+)}\right\}^{-1}, \tag{5}$$

where we have taken $\alpha = 0\cdot984$ and the oscillator strength f from Goldwire's (1968) tables. Solving for T_{e}, we obtain the values given in column 4 of Table 4. These are close to those calculated from equation (4) but are all somewhat less (by an average of about 5%). For the Orion Nebula the value is 16% lower.

Gordon and Meeks (1967) showed that the electron temperature could be calculated from hydrogen and helium data by assuming that the turbulent velocity is the same for both. They thus derived the expression

$$T_{\mathrm{e}} = \frac{c^2}{8k\ln2}\left(\frac{1}{M_{\mathrm{H}}}-\frac{1}{M_{\mathrm{He}}}\right)^{-1}\left\{\left(\frac{\Delta\nu_{\mathrm{H}}}{\nu_{\mathrm{H}}}\right)^2-\left(\frac{\Delta\nu_{\mathrm{He}}}{\nu_{\mathrm{He}}}\right)^2\right\}, \tag{6}$$

where M_{H} and M_{He} are the masses of the hydrogen and helium atoms. As seen in column 5 of Table 4, values of T_{e} derived from equation (6) are very much higher than those from the two previous formulae. With the strong dependence in (6) on the term involving the squares of the half-widths, the accuracy of the measurements is most important. To illustrate: if the half-width of the helium line in NGC 2024 were at the upper extreme of the quoted errors, i.e. 455 kHz instead of 355 kHz, then T_{e} would change from 12 097 K to 9397 K. The ratio of half-widths (H to He) would have to be reduced by 33% for values from equation (6) to agree with values from equations (4) and (5). It may be noted that the exceptionally high values of T_{e} are for sources with H 90α half-widths well above 1 MHz (Table 2*a*). These then must be either exceptional HII regions or else the widths have been produced by partial superpositions of several HII regions at different radial velocities.

If T_{e} values from equation (4) are adopted in the relation (discussed by e.g. Kardashev 1959) in which the thermal and turbulent contributions are separated, then the turbulent velocity V_{t} in the nebula is given by

$$V_{\mathrm{t}}^2 = \frac{3}{2}\frac{(\Delta\nu)^2 c^2}{4\nu_{\mathrm{H}}^2\ln2} - \frac{3kT_{\mathrm{e}}}{M_{\mathrm{H}}}. \tag{7}$$

The values of V_{t} derived in this way are listed in column 3 of Table 4. They lie in the range 10–30 km s^{-1}, in agreement with values found by other authors. However, if equation (6) is used for T_{e}, the derived values of the turbulent velocity (column 6 of Table 4) are much less, falling in the range 1–20 km s^{-1}.

Lines of Elements Heavier than Helium

For the sources Orion Nebula, RCW 38, 1441 − 59, 1608 − 51 and Omega Nebula, gaussian fitting to the 100 kHz spectra indicates the presence of an extra component near 8876·7 MHz which, for reasons given in Section 4, we have called Li 90α. In four of these sources the radial velocities were within 0·1 km s^{-1} of those of the H 90α lines; in the case of 1441 − 59 the difference was 0·5 km s^{-1}.

For each of the sources RCW 38, 1441 − 59 and 1608 − 51 a further component is needed which, if identified as C 90α, has a radial velocity within $0\cdot1$ km s^{-1} of the corresponding H 90α line. The C 90α line in NGC 2024 at a radial velocity of $+10\cdot2$ km s^{-1} is in agreement with the results of other observers. The corresponding line in 1109 − 610 is within $0\cdot1$ km s^{-1} of the H 90α velocity ($-24\cdot1$ km s^{-1}) for that source.

In several other cases the Li or C lines have been fitted by the GAUFIT program at velocities close to the H lines, but since the intensities are below the noise level of the observations the results cannot be taken seriously. These sources are RCW 36, 1112 − 609, Norma I and Norma II.

We regard the measurements and results discussed in this subsection as extremely provisional.

Radial Velocities of Ionized and Molecular Gases in Directions of Sources

Table 2*b* shows that, for more than half the sources in this survey, the radial velocities of the ionized gases (H, He, ...) and the molecular gases are nearly equal. At least one of the absorption velocities in either formaldehyde (H_2CO) or hydroxyl (OH) is less than $1\cdot7$ km s^{-1} from the recombination line velocity for each of the following 10 sources: RCW 38, RCW 36, RCW 49, 1109 − 610, 1112 − 610, 1441 − 59, 1608 − 51, Norma III, Sgr B2 and Omega Nebula. It is reasonable to conclude that the molecular gases are in close proximity to the nebulae in these cases. Velocity differences in the range $2\cdot7$–$4\cdot4$ km s^{-1} for the nebulae NGC 2024, Car I, Norma I and Norma II indicate some proximity of the molecular gases. For the Orion Nebula the difference is $8\cdot2$ km s^{-1}, but explanatory models have been put forward in this case (see e.g. Zuckerman 1973). The cases of Car II and 1112 − 609 are confused because of angular resolution difficulties at frequencies less than $8\cdot9$ GHz on the 64 m telescope.

7. Conclusions

This survey of 17 southern nebulae for recombination lines near a frequency of $8\cdot9$ GHz has supplied evidence that the α, β and γ lines of hydrogen and the helium lines arise in the same region of the nebula. We have shown that the abundance ratio $N(He^+)/N(H^+)$ of singly ionized helium to ionized hydrogen varies between $0\cdot02$ and $0\cdot10$ and that, as would be expected, the helium line has a smaller half-width than the corresponding hydrogen line. The observations have further underlined the difficulty of obtaining satisfactory values for electron temperature and turbulent velocity from radio recombination lines.

With the additional information on the spectrum near the helium line provided by these observations it seems that the simple approach of attributing additional higher frequency lines to carbon (at whatever radial velocity is needed) should be carefully reconsidered.

Acknowledgments

We are grateful to Mr P. W. Butler for his efforts in the setting up and maintenance of the receiver and the associated cryogenic system. Mr J. X. McGee, School of Electrical Engineering, University of Sydney, assisted with many of the observations.

References

Chaisson, E. J. (1973*a*). *Astrophys. J.* **182**, 767–80.
Chaisson, E. J. (1973*b*). *Astrophys. J.* **186**, 545–53.
Chaisson, E. J., and Ball, J. A. (1971). *Astrophys. J.* **169**, 495–501.
Chaisson, E. J., and Lada, C. J. (1974). *Astrophys. J.* **189**, 227–37.
Churchwell, E., and Mezger, P. G. (1970). *Astrophys. Lett.* **5**, 227–31.
Doherty, L. H., Higgs, L. A., and Macleod, J. M. (1972). *Astrophys. Lett.* **12**, 91–8.
Gardner, F. F., Milne, D. K., Mezger, P. M., and Wilson, T. L. (1970). *Astrophys. Lett.* **6**, 87–91.
Goldwire, H. C. (1968). *Astrophys. J. Suppl. Ser.* **17**, 445–566.
Gordon, M. A., and Meeks, M. L. (1967). *Astrophys. J.* **149**, L21–5.
Hjellming, R. M., and Davies, R. D. (1970). *Astron. Astrophys.* **5**, 53–67.
Hjellming, R. M., and Gordon, M. A. (1970). *Astrophys. J.* **164**, 47–60.
Kardashev, N. S. (1959). *Astron. Zh.* **36**, 838–44.
Kellermann, K. I., and Pauliny-Toth, I. I. K. (1971). *Astrophys. Lett.* **8**, 153–60.
Kerr, A. R. (1971). CSIRO Div. Radiophys. Internal Rep. No. RPL 185.
Lada, C. J., and Chaisson, E. J. (1973). *Astrophys. J.* **183**, 479–89.
McGee, R. X., and Gardner, F. F. (1968). *Aust. J. Phys.* **21**, 149–66.
Menzel, D. H. (1968). *Nature* (*London*) **218**, 756–7.
Mezger, P. M., Wilson, T. L., Gardner, F. F., and Milne, D. K. (1970). *Astron. Astrophys.* **6**, 35–7.
Robbins, R. R., Daltabuit, E., and Cox, D. P. (1971). *Astrophys. J.* **169**, L77–81.
Traub, W. A., and Carleton, N. P. (1973). *Astrophys. J.* **184**, L11–14.
Vanden Bout, P. A., and Grupsmith, G. (1974). *Astrophys. J.* **187**, L9–11.
Waltman, E. B., and Johnson, K. J. (1973). *Astrophys. J.* **182**, 489–96.
Whiteoak, J. B., and Gardner, F. F. (1975). The 4830 MHz formaldehyde absorption in the direction of galactic radio sources. *Astron. Astrophys.* (in press).
Wilson, T. L., Mezger, P. G., Gardner, F. F., and Milne, D. K. (1970). *Astron. Astrophys.* **6**, 364–84.
Zuckerman, B. (1973). *Astrophys. J.* **183**, 863–9.
Zuckerman, B., and Ball, J. A. (1974). *Astrophys. J.* **190**, 35.

Manuscript received 30 September 1974